JGR Atmospheres

RESEARCH ARTICLE
10.1029/2025JD044324

Impacts of Local and Remote Sub-Grid Terrain Solar Radiative Effect on the Meiyu Rainfall Forecast in the Yangtze-Huaihe River Basin, China

Shuxin Cai[1], Kefeng Zhu[2], Anning Huang[3], Chunlei Gu[3], Yang Wu[2,4], Xinsheng Zhu[5], and Wei Zhao[5]

[1]Zhejiang Meteorological Service Center, Hangzhou, China, [2]Nanjing Innovation Institute for Atmospheric Sciences, Chinese Academy of Meteorological Sciences–Jiangsu Meteorological Service, Nanjing, China, [3]School of Atmospheric Sciences, Nanjing University, Nanjing, China, [4]Jiangsu Key Laboratory of Severe Storm Disaster Risk / Key Laboratory of Transportation Meteorology of CMA, Nanjing, China, [5]Nanjing Institute of Environmental Sciences, Ministry of Ecology and Environment of the People's Republic of China, Nanjing, China

Key Points:

- The overestimated Meiyu rainfall can be obviously reduced by considering the sub-grid terrain solar radiative effect (STSRE)
- The STSRE of Tibetan Plateau weakens the Meiyu rainfall by remotely suppressing the ascending motion in the Yangtze-Huaihe River region
- The STSRE of Yangtze-Huaihe River region largely improves the Meiyu rainfall forecast by locally weakening the water vapor transport there

Correspondence to:
K. Zhu and A. Huang,
zhukf@cma.gov.cn;
anhuang@nju.edu.cn

Citation:
Cai, S., Zhu, K., Huang, A., Gu, C., Wu, Y., Zhu, X., & Zhao, W. (2025). Impacts of local and remote sub-grid terrain solar radiative effect on the Meiyu rainfall forecast in the Yangtze-Huaihe River Basin, China. *Journal of Geophysical Research: Atmospheres*, *130*, e2025JD044324. https://doi.org/10.1029/2025JD044324

Received 13 MAY 2025
Accepted 2 NOV 2025

Author Contributions:
Conceptualization: Anning Huang
Data curation: Shuxin Cai, Chunlei Gu
Formal analysis: Shuxin Cai
Investigation: Shuxin Cai, Kefeng Zhu, Chunlei Gu, Yang Wu, Xinsheng Zhu, Wei Zhao
Methodology: Shuxin Cai, Kefeng Zhu, Anning Huang, Chunlei Gu
Project administration: Anning Huang
Resources: Shuxin Cai, Kefeng Zhu, Chunlei Gu
Supervision: Anning Huang
Validation: Kefeng Zhu, Yang Wu, Wei Zhao
Visualization: Shuxin Cai
Writing – original draft: Shuxin Cai
Writing – review & editing: Kefeng Zhu, Anning Huang, Chunlei Gu, Yang Wu, Xinsheng Zhu, Wei Zhao

Abstract Including the sub-grid terrain solar radiative effect (STSRE) of East Asia in the convection-permitting Weather Research and Forecasting model can clearly improve the forecast skill of Meiyu rainfall in the Yangtze-Huaihe River Basin (YHRB). However, the STSRE of which region mainly leads to the improvement of Meiyu rainfall forecast remains unclear. This study systematically explores the impacts of local and remote STSRE on the Meiyu rainfall forecast, their relative importance, and underlying physical mechanisms. Results show that relative to the remote STSRE of Tibetan Plateau (TP), the local STSRE of YHRB leads to relatively larger improvement of Meiyu rainfall forecast with the root mean square error decreased by 6.24% and Taylor score increased by 2.76%. Further mechanism analysis indicates that the STSRE of the TP weakens the TP heat source, leading to weakening and westward shifting of the South Asian High, which in turn suppresses the divergence in the upper troposphere and the ascending motion over the YHRB and thereafter improves Meiyu rainfall forecast. In contrast, the STSRE of the YHRB decreases surface incident solar radiation and surface thermal conditions, producing a cold anomaly and anticyclonic circulation difference in the lower troposphere over the YHRB. This anticyclonic difference directly weakens southwesterly water vapor transport, thereby reducing the overestimation of Meiyu rainfall. This study highlights the importance of local terrain (rather than the TP) in enhancing Meiyu rainfall forecast accuracy for 3–4 days weather forecasts.

Plain Language Summary The topography of China is complex, featuring plateaus, mountains, and hills. The sub-grid terrain solar radiative effect (STSRE) not only influences the simulations of land surface processes and precipitation in the Tibetan Plateau (TP) but also affects those in downstream regions. However, the physical mechanism and evolution process of how the STSRE in different regions regulate the precipitation forecast in the plain regions remain unclear. This study explores the impacts of local and remote STSRE on the Meiyu rainfall forecast in the Yangtze-Huaihe River Basin (YHRB). Results show that the STSRE of TP remotely suppresses the divergence in the upper troposphere and ascending motion in the lower troposphere over the YHRB to improve the Meiyu rainfall forecasts. In contrast, the decrease of the surface incident solar radiation and surface thermal condition induced by the local STSRE of YHRB leads to a local cold anomaly in the lower troposphere, which directly weakens the southwesterly water vapor transport, finally reducing the overestimation of Meiyu rainfall. Overall, the local terrain (rather than the TP) plays a crucial role in reducing such overestimation during 3–4 days weather forecasts.

1. Introduction

The Meiyu rainfall is the product of the northward movement of the East Asian summer monsoon, which is the main precipitation system in the Yangtze-Huaihe River Basin (YHRB) during summer (Ding, 1992; Ding & Chan, 2005; Ding et al., 2021; Tao & Chen, 1987; Zeng et al., 2022). Previous studies have shown that convection-permitting models can reproduce the general pattern of the Meiyu rainband (Guo et al., 2020; Jin et al., 2016; Luo & Chen, 2015; Xu et al., 2021; Xue et al., 2018). However, the Meiyu rainfall is significantly overestimated, both in terms of extreme values and in the spatial extent of heavy rainfall (Li et al., 2020; Yun et al., 2020; Zhu et al., 2018).

As shown in previous studies, the Tibetan Plateau (TP) could affect Meiyu rainfall systems by changing the surrounding atmospheric circulation through its dynamic and thermal effects (Wang et al., 2009; Xu et al., 2010). Also, the low vortices and shear lines originating from the TP are closely related to the heavy precipitation during Meiyu rainfall period (Chen et al., 2015; Wu et al., 2020; Xu et al., 2000). Thus, accurate representation of weather and climate over the TP is essential for Meiyu rainfall forecasts and simulations (Ma et al., 2022). Shi et al. (2024) found that the overestimation of Meiyu rainfall is associated with overestimated southwesterly winds, resulting in more water vapor transported to the YHRB, thereby producing excessive precipitation. Further analysis indicates that the warm bias over the TP and the cold bias in southeastern China enhance the air temperature gradient from northwest to southeast, leading to the overestimated southwesterly winds. The warm bias over TP may take 2–3 days to affect the YHRB while the cold bias can induce a local cold high pressure, generating an anticyclonic wind bias that intensifies the southwesterly flow, leading to overestimated Meiyu rainfall in YHRB. Similar conclusions have also been mentioned in study of Hu et al. (2024). Although these studies proposed a possible mechanism, they did not validate it through sensitivity experiments.

A recent study of Cai et al. (2023) showed that adopting a three-dimensional sub-grid terrain solar radiative effect (STSRE) scheme developed by Huang et al. (2022) into the convection-permitting Weather Research and Forecasting model (WRF_CPM) can effectively reduce the warm bias over TP. The reduced TP heating weakens the southwesterly winds, thereby reducing the convergence of moisture flux over the southern TP. Moreover, the weakened thermal low stabilizes the local atmosphere and suppresses the local convection. These effects greatly alleviate the overestimation of precipitation over the southern TP produced by the WRF_CPM without considering the STSRE. They also pointed out that including the STSRE scheme can improve the downstream Meiyu precipitation forecast, but the underlying causes and mechanisms were not discussed in that study. Most previous studies on how the STSRE over the TP influences downstream regions primarily focus on long-term climate simulations (Gu et al., 2020; Hao et al., 2023; Lee et al., 2019; Zhang et al., 2024). Since these simulations span several months to several years, the TP's thermal effects have sufficient time to influence downstream regions (Chen et al., 2015; Duan et al., 2012; Shi & Wen, 2015; Wu et al., 2007; Xu et al., 2002). Gu et al. (2020) indicated that the STSRE can greatly reduce the warm bias over the TP, thereby reducing the land-sea thermal contrast at a large scale and thereafter weakening the East Asian summer monsoon, and ultimately improving the Meiyu precipitation simulations at a long-term scale.

However, in weather forecasting, the forecast period is typically 3–4 days, prompting the question of how the improvements of TP's thermal condition forecasts influence the Meiyu rainfall forecast in the downstream YHRB within such a short forecast period. Moreover, the YHRB contains numerous small- to medium-scale terrain, including the Wuyi Mountains and Dabie Mountains, whose radiation budgets are also affected by the STSRE. How the local STSRE affects the Meiyu rainfall forecasts over the YHRB remains unclear. The purpose of this study is to figure out to what extent the remote STSRE of TP and local STSRE of YHRB can mitigate the Meiyu precipitation overestimation and to clarify their influencing mechanisms. We will focus on addressing the following scientific questions: How do the local STSRE and remote STSRE affect the Meiyu precipitation forecasts? What is their relative importance? And what are the possible underlying mechanisms? The findings of this study may deepen the understanding of the roles of STSRE from different regions in improving the Meiyu rainfall forecasts.

The rest of this paper is organized as follows: In Section 2, we briefly introduce the WRF_CPM and the STSRE scheme, as well as the observation data, experimental design, and the evaluation metrics. Then, how the STSRE scheme affects the performance of WRF_CPM to forecast the Meiyu precipitation in the YHRB is presented in Section 3. Section 4 indicates the influences of the local and remote STSRE on the Meiyu precipitation forecast, their relative importance, and underlying physical mechanisms. The conclusions are given in Section 5.

2. Model, Data, Experimental Design, Method

2.1. Model

In this study, we used the WRF version 4.2 model with a horizontal resolution of convection-permitting (~4 km), which is called as WRF_CPM. It can well portray the spatial distribution of the complicated terrains at model grid scale, but the impact of sub-grid terrain features on the surface downward solar radiation (SDSR) cannot be described by the current plane-parallel radiation scheme. To depict the STSRE more realistically, a three-dimensional STSRE (3D-STSRE) scheme developed by Huang et al. (2022) has been incorporated into the

Table 1
Details of Data Sets

Name	Variable	Temporal resolution	Spatial resolution
SRTM	Terrain elevation	/	3″ (~90 m)
East Asia-Pacific longwave/shortwave downward radiation data set	SDSR	10-min	0.05° × 0.05°
CMA rain gauge and CMORPH combined data set	precipitation	1-hr	0.05° × 0.05°
NCEP-GFS	All forecast variables	3-hr	0.25° × 0.25°

WRF_CPM (Cai et al., 2023). Compared with the plane-parallel radiation scheme, the 3D-STSRE scheme fully considers the impact of 3D structure (terrain slope and aspect, sky view factor, shadowing and reflecting effects of nearby terrains) of the sub-grid terrains on the SDSR within a given model grid, and can significantly improve the SDSR simulations over rugged areas (Gu et al., 2024; Zhang et al., 2022, 2024). Study of Cai et al. (2023) indicates that adopting the 3D-STSRE scheme in the WRF_CPM can greatly alleviate the overestimation of SDSR and precipitation by weakening the surface heating in the TP region with complicated terrains.

2.2. Data

The data sets used in this study are as follows:

1. To incorporate the 3D-STSRE scheme into the WRF_CPM, the sub-grid topographic parameters are needed. These parameters are based on the digital elevation model data. We used the Shuttle Radar Topography Mission data of 3″ (~90 m) (Jarvis et al., 2008) to figure the sub-grid terrain parameters.
2. The East Asia-Pacific longwave/shortwave downward radiation data are utilized to evaluate the SDSR produced by the model. This data set is derived from the Himawari-8 geostationary satellite data with considering effects of factors such as clouds, aerosols, and terrains (Letu et al., 2022). It shows high accuracy when compared with ground observations in the East Asia region.
3. The China Meteorological Administration rain gauge and Climate Prediction Center's morphing technique (CMORPH; Joyce et al., 2004) merged data set is used to assess the Meiyu rainfall forecast. Preceding studies implied that this merged rainfall product could provide detailed rainfall features and exhibit smaller systematic biases and root mean squared errors versus the original CMORPH data set (Li et al., 2021; Shen et al., 2014; Wu et al., 2018). This data set is dependable for analysis of annual and summer precipitation in both plain and complicated regions of China (Cai et al., 2021; Yu et al., 2020; Zhu et al., 2021).
4. The initial and lateral boundary conditions of WRF_CPM in each experiment are derived from the NCEP Global Forecast System (NCEP-GFS) real-time forecast data (NCEP, 2015).

The details of each data can be found in Table 1.

2.3. Experimental Design

To determine whether the enhanced accuracy of Meiyu rainfall forecasts results from the STSRE in the TP region or the STSRE within the YHRB, we carried out 4 sets of numerical experiments. Figure 1 shows the spatial distribution of where the STSRE is enabled in the sensitive experiments, using the sky view factor (SVF) as an example. The relatively lower SVF indicates much more complex terrain (Huang et al., 2022). The details of each experiment are shown as follows: (a) the CTRL experiment with the WRF_CPM adopting the plane-parallel radiation scheme in the whole model domain, (b) the STSRE_ALL experiment with WRF_CPM adopting the 3D-STSRE scheme in the whole domain (Figure 1a), (c) the STSRE_TP experiment with the 3D-STSRE scheme (plane-parallel radiation scheme) activated in the TP region indicated by the shadings (other regions of the model domain) (Figure 1b), and (d) the STSRE_YHRB experiment with the 3D-STSRE scheme (plane-parallel radiation scheme) activated in the YHRB indicated by the shadings (other regions of the model domain) (Figure 1c). For all of the experiments, the model domain covers the entire China and has 1,408 × 1,080 in horizontal direction and 50 layers in vertical direction. The horizontal resolution is set to 4 km.

Three Meiyu rainfall episodes in 2020 were selected for testing. These rainfall centers were primarily located in the YHRB, characterized by substantial precipitation amounts (Zeng et al., 2022). Each of the three events spans 96 hr. The forecast periods are from 00:00 UTC on 10 June to 00:00 UTC on 14 June 2020, from 00:00 UTC on 18

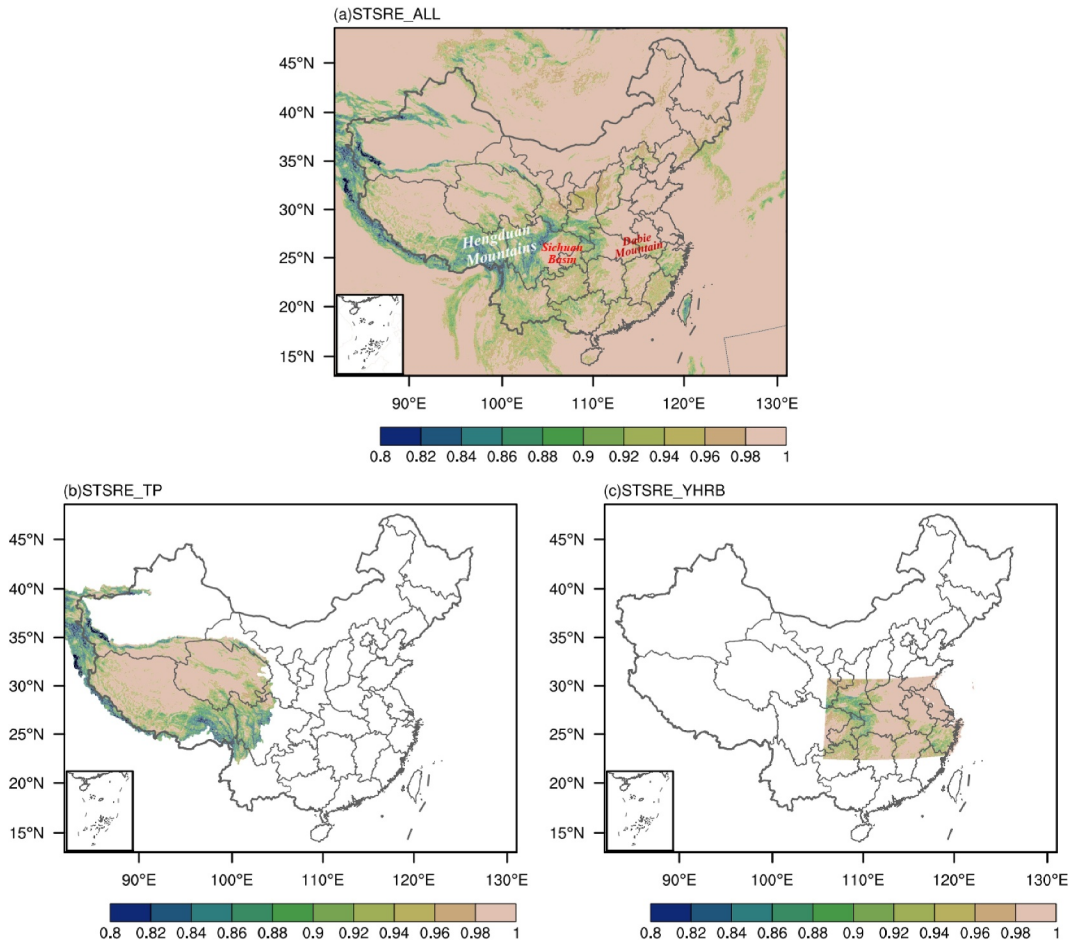

Figure 1. The spatial distribution of where the sub-grid terrain solar radiative effect (STSRE) is activated in the STSRE_ALL experiment (a), STSRE_TP experiment (b), and STSRE_YHRB experiment (c) using the sky view factor (SVF, shadings) as an example.

June to 00:00 UTC on 22 June 2020, and from 00:00 UTC on 28 June to 00:00 UTC on 1 July 2020, respectively. In all of the experiments, the WRF_CPM utilizes the same physical parameterization configuration as follows: the Yonsei University planetary boundary layer scheme (YSU; Hong et al., 2006), the NOAH land surface model (Chen & Dudhia, 2001), the CAM shortwave and longwave radiation schemes (Collins et al., 2004), and the WRF Single-Moment 5-class microphysics (WSM5; Hong et al., 2004). We used NCEP-GFS real-time forecast data (NCEP-GFS; NCEP, 2015) as the initial and lateral boundary conditions of WRF_CPM. To explore the time evolution of the remote and local impacts of STSRE on the Meiyu rainfall forecast, the hourly output data of all the 96 hr for each rainfall process are used for analysis.

2.4. Method

Four statistical metrics were used to assess the model performance: the mean bias (MB), the relative error, the RMSE, and the Taylor score (TS; Taylor, 2001). Mean bias represents the arithmetic mean error between the model results and the observations. Relative error is the percentage form of the deviation between the model and observations, which can reflect the model bias more intuitively. Root mean squared error indicates the degree of deviation of the model results compared with the observation. The smaller RMSE indicates the better model performance. TS ranging from 0 to 1 denotes the model ability in simulating the amplitude and variability of observations, higher TS implies better skill. The detailed calculations of these metrics are given as follows:

$$\mathrm{MB} = \frac{1}{n}\sum_{i=1}^{n}(M_i - O_i) \tag{1}$$

$$\mathrm{RE} = \frac{\overline{M} - \overline{O}}{\overline{o}} \times 100\% \tag{2}$$

$$\mathrm{RMSE} = \sqrt{\frac{1}{n}\sum_{i=1}^{n}(M_i - O_i)^2} \tag{3}$$

$$\mathrm{TS} = \frac{4(1+R)}{\left(\sigma + \frac{1}{\sigma}\right)^2 (1+R_0)} \tag{4}$$

$$R = \frac{\sum_{i=1}^{n}\left(M_i - \overline{M}\right)\left(O_i - \overline{O}\right)}{\sqrt{\sum_{i=1}^{n}\left(M_i - \overline{M}\right)^2}\sqrt{\sum_{i=1}^{n}\left(O_i - \overline{O}\right)^2}} \tag{5}$$

Where M_i (O_i) represents the simulation (observation) at the ith point. $\overline{M}$ ($\overline{O}$) are the mean value of simulations (observations) for the n samples. σ is the standard deviation of simulations normalized by that of observations. R is the correlation between simulations and observations. As an achievable maximum correlation, R_0 is set to 1.

Additionally, the bootstrap resampling technique is used to estimate the confidence intervals (Pan et al., 2014; Wu et al., 2025). In all cases, the bootstrapped estimates are generated using nBoot = 1,000. For these samples, their mean and a two-tailed 90% confidence interval is calculated. When the bounds of a 90% confidence interval for RMSE (TS) percentage changes lie entirely below (above) zero, it indicates that the improvement resulting from the sensitive experiment relative to the CTRL experiment is statistically significant at the 90% confidence level. Conversely, if the interval includes zero, the improvement is not statistically significant (Pan et al., 2014).

3. Model Evaluation

3.1. Impact of the STSRE on the SDSR Forecast

Figure 2 shows the distribution of the observed and forecasted SDSR and the SDSR differences during the three rainfall events in June 2020. As shown in Figure 2a, strong SDSR can be observed in the central and western TP region with higher altitude, where the air is thin and has a much weaker attenuation effect on the SDSR; however, the magnitude of SDSR in the Meiyu rainfall region and Sichuan Basin is much weaker due to the frequent rainfall and thick clouds. Compared with the observation, the CTRL experiment generally reproduces the distribution of SDSR, but overestimates the SDSR in most areas, with the largest bias up to 100 W m^{-2} (Figures 2b and 2d). With the application of 3D-STSRE scheme in the STSRE_ALL experiment, the overestimation of SDSR over the Sichuan Basin and YHRB in the CTRL experiment (Figure 2d) can be clearly reduced by up to 40 W m^{-2} (Figure 2f).

Figure 3 further gives the MB and RMSE of the SDSR in the regions with different SVF categories produced by the two experiments. The grids with SVF less than 0.85 are generally distributed in the regions with complicated terrain (Figure 1a). The CTRL experiment can roughly reproduce the SDSR distribution. However, it overestimates the SDSR under all SVF categories (Figure 3a). The MB and RMSE of SDSR produced by the CTRL experiment are larger in the rugged regions with smaller SVF (Figures 3a and 3b). With the adoption of STSRE scheme in the STSRE_ALL experiment, the overestimation of SDSR under each category of SVF in the CTRL experiment is mitigated and the improvement is much more noticeable at the grids with smaller SVF (Figures 3a and 3b). When the SVF < 0.8, the RMSE (MB) of SDSR simulated by the CTRL experiment can be reduced by 28 W m^{-2} (35 W m^{-2}) by the adoption of STSRE scheme. Although RMSE improvement is smaller in plain regions (SVF ≥ 0.97) than in rugged regions (SVF < 0.97), the reduction remains between 6 and 8 W m^{-2} (Figure 3b).

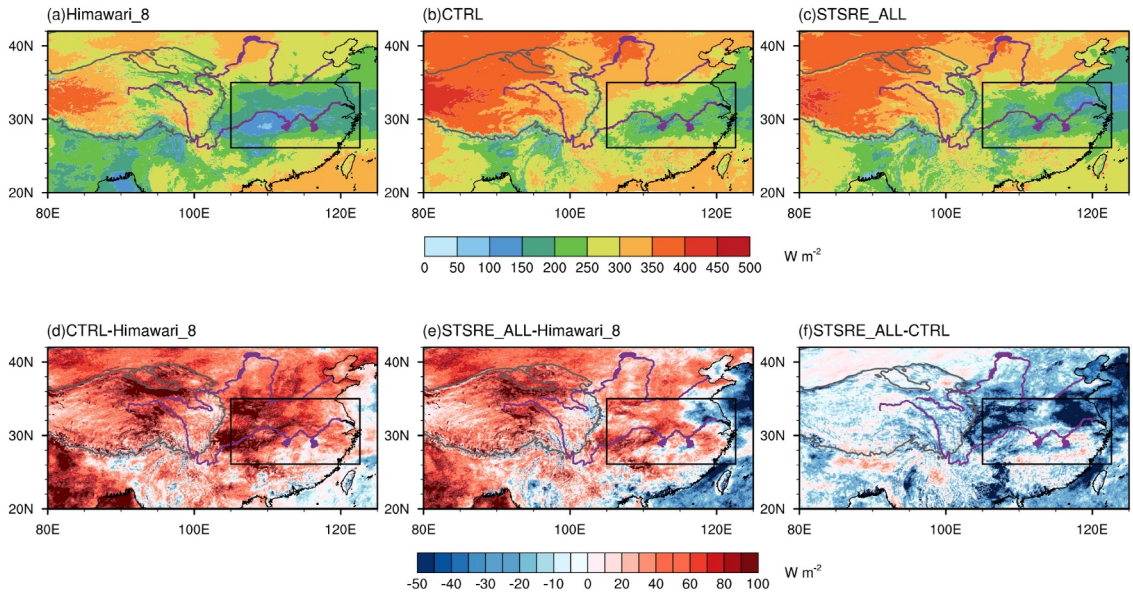

Figure 2. The mean surface downward solar radiation (SDSR) from the Himawari-8 observations (a), predictions of the CTRL (b), and STSRE_ALL (c) experiments during the three Meiyu rainfall events in June 2020. The mean SDSR differences between the CTRL experiment and Himawari-8 (d), between the STSRE_ALL experiment and Himawari-8 (e) and between the STSRE_ALL and CTRL experiments (f) during the three Meiyu rainfall events in June 2020, respectively. The gray solid lines denote the Tibetan Plateau region and the purple solid lines indicate the Yangtze River and Yellow River. The black rectangles denote the Yangtze-Huaihe River Basin.

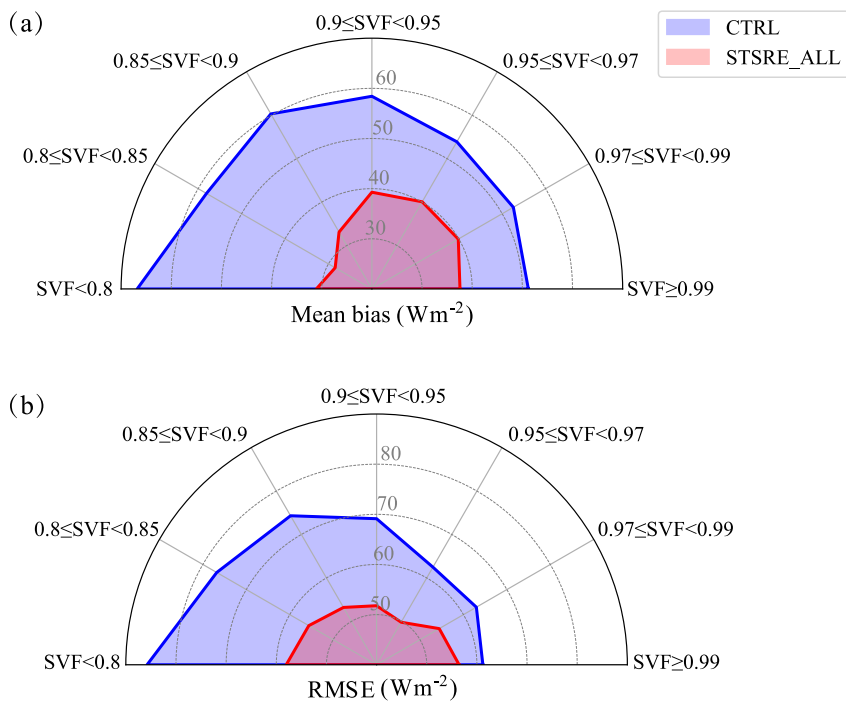

Figure 3. The biases (a) and root mean square errors (b) of the mean surface downward solar radiation forecasted by the CTRL and STSRE_ALL experiments against the Himawari-8 observations during the three rainfall events in June 2020 averaged within each category of SVF.

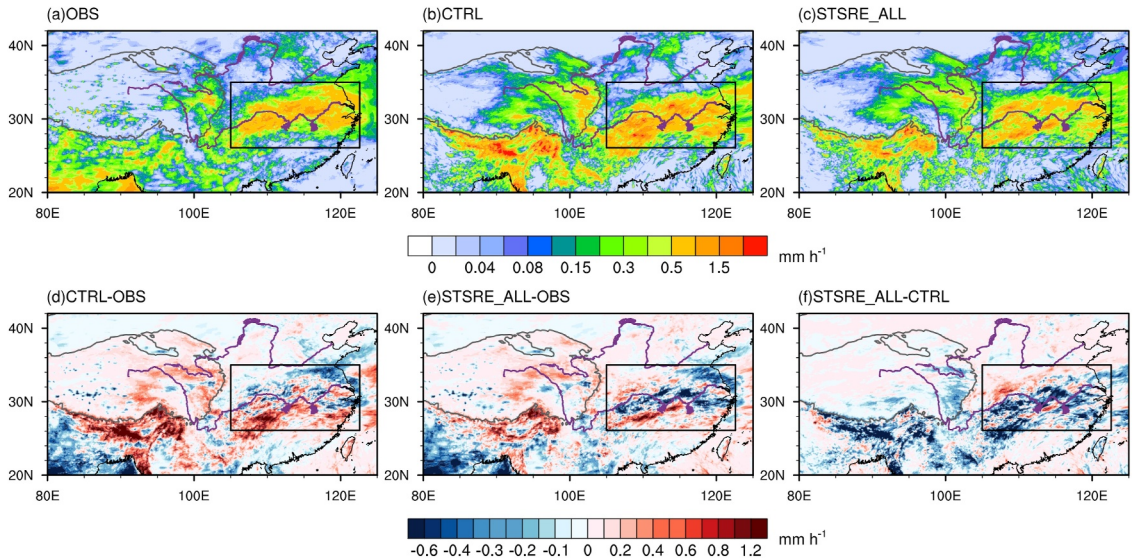

Figure 4. The mean precipitation from the observations (a) and simulations from CTRL (b) and STSRE_ALL (c) experiments during the three Meiyu rainfall events in June 2020. The mean precipitation differences between CTRL and observation (d), between STSRE_ALL experiment and observation (e) and between STSRE_ALL and CTRL experiments (f) during the three Meiyu rainfall events in June 2020. The gray lines denote the Tibetan Plateau region and the purple solid lines indicate the Yangtze River and Yellow River. The black boxes represent the Yangtze-Huaihe River Basin.

3.2. Impact of the STSRE on the Meiyu Rainfall Forecast

As illustrated in Figure 4a, the observed precipitation mainly locates at eastern TP region and YHRB, with the maximal mean precipitation during the three Meiyu rainfall events in June 2020 up to 1.5 mm hr^{-1}. Compared with the observation, the CTRL experiment can reproduce the rainfall distribution in the YHRB (Figure 4b). However, it produces much more (less) precipitation over southern (northeastern) YHRB (Figure 4d). The adoption of 3D-STSRE scheme in the STSRE_ALL experiment can clearly reduce precipitation biases produced by the CTRL experiment in most parts of the YHRB (Figure 4f). Due to the application of 3D-STSRE scheme, the MB and RMSE of Meiyu rainfall forecast over the YHRB can be reduced by 31.48% and 10.43%, respectively.

Figure 5 further shows the time series of the RMSE of each precipitation event in the YHRB produced by the CTRL and STSRE_ALL experiments. We calculated the RMSE of each grid point of three Meiyu rainfall events in the YHRB and then took the average of three events. Results show that for all three events, the STSRE_ALL experiment demonstrates lower RMSE values compared with the CTRL experiment. In the earlier stage of forecast, the RMSEs of precipitation produced by the two experiments are close to each other. For Events 1 and 3, the STSRE_ALL experiment shows consistently lower RMSE than the CTRL experiment after 12 hr. For Event 2, the RMSE improvement becomes particularly evident after 40 hr. These findings suggest that the influence of STSRE on Meiyu rainfall forecast requires a certain response time to manifest clearly.

As the analysis above, consideration of the STSRE in East Asia can obviously improve the Meiyu rainfall forecast in the YHRB (Figure 4f); however, the STSRE of which region mainly leads to the improvement of Meiyu rainfall forecast remains unclear. In addition to the strong STSRE in the TP with complex terrains, the STSRE can also induced by the mountains and hills in the YHRB (Figure 1a). To identify whether the improvement of Meiyu rainfall forecast comes from the remote STSRE of the TP or the local STSRE of the YHRB, two sensitive experiments were carried out using WRF_CPM with the 3D-STSRE scheme applied only in the TP (Figure 1b) or YHRB (Figure 1c).

Figure 6 displays the differences of Meiyu rainfall forecast between sensitive experiments and the CTRL experiment over the YHRB. We can observe a large area of precipitation reduction in both the STSRE_ALL and STSRE_YHRB experiments (Figures 6a and 6c), whereas the STSRE_TP experiment shows a large area of increased precipitation in the south of YHRB (Figure 6b). The spatial pattern of rainfall differences in STSRE_YHRB resembles that in STSRE_ALL more closely than in STSRE_TP. This indicates that the reduction

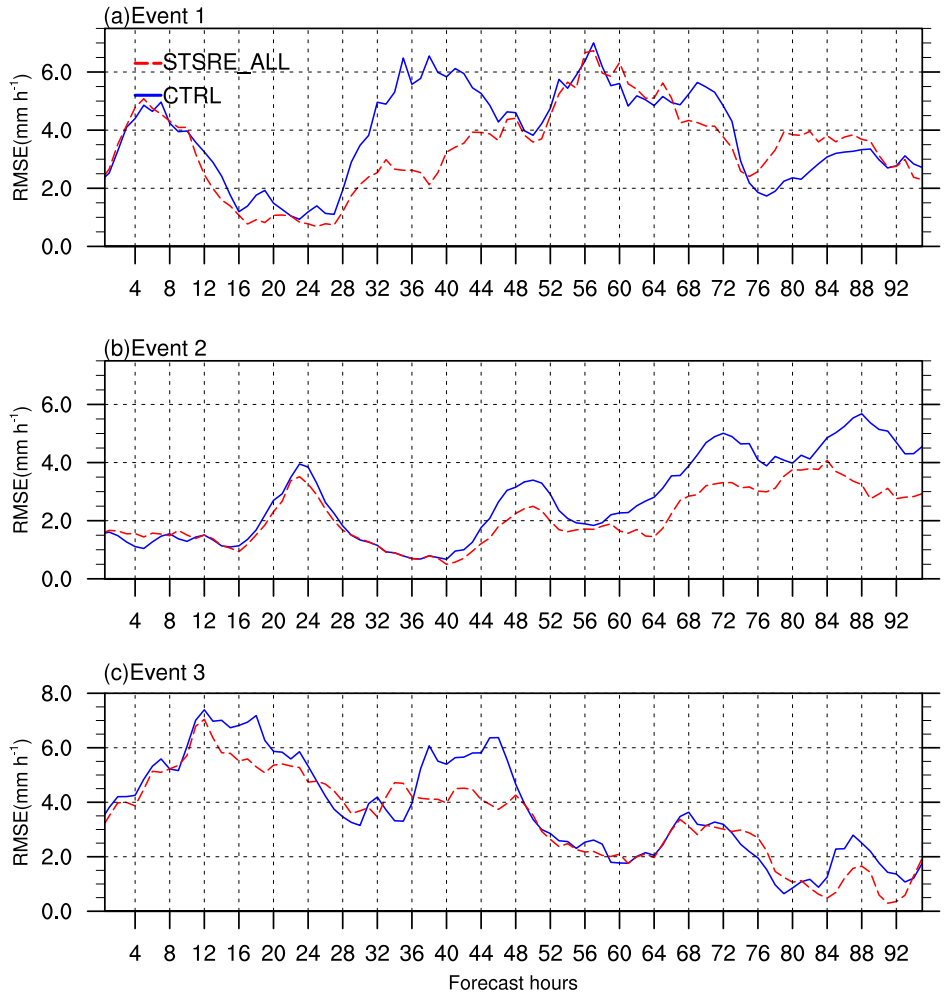

Figure 5. Time series of the root mean squared error (RMSE) of each precipitation event forecasted by the CTRL and STSRE_ALL experiments against the observation during June 2020 regionally averaged over the precipitation center in the Yangtze-Huaihe River Basin region.

in Meiyu precipitation is primarily driven by the STSRE of the YHRB region. The results align well with the subsequent physical mechanism explaining the contributions of remote TP and local terrain effects.

To quantify the relative importance of STSRE in the TP and YHRB to the improvement of Meiyu rainfall forecast, we calculated the TS and RMSE of the rainfall forecasted by all experiments against the observation. The percentage changes of the RMSE and TS of precipitation produced by each sensitive experiment relative to the CTRL experiment were also revealed. In general, the RMSEs (TSs) produced by three sensitive experiments are lower (higher) than the CTRL experiment at the 90% confidence level (see the percentage change in the bottom panel of Figure 7), implying that the adoption of STSRE scheme can well improve the Meiyu rainfall forecast. Compared with the CTRL experiment, the percentage changes of RMSE and TS of precipitation produced by the STSRE_YHRB experiment are 6.24% and 2.76%, respectively. However, the changes of RMSE and TS of precipitation produced by the STSRE_TP experiment are only 2.25% and 0.6%, respectively. This suggests the improvement of the Meiyu precipitation forecast induced by the local STSRE in the YHRB is much higher than that resulted from the remote STSRE in the TP.

4. Physical Mechanisms

The following section will discuss the mechanisms of how the local (remote) STSRE in the YHRB (TP) affects the Meiyu rainfall forecast and the evolution processes. Figure 8 illustrates the evolution of SDSR deviations

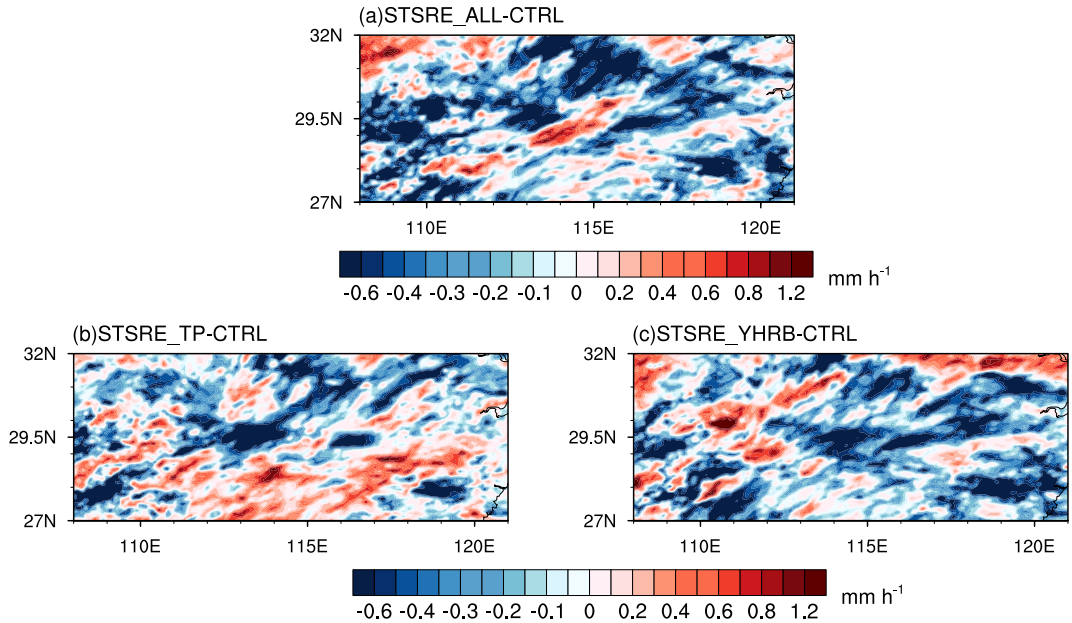

Figure 6. The mean rainfall differences between the STSRE_ALL and CTRL experiments (a), STSRE_TP and CTRL experiments (b), and between STSRE_YHRB and CTRL experiments (c) in the Yangtze-Huaihe River Basin region during three rainfall events in June 2020.

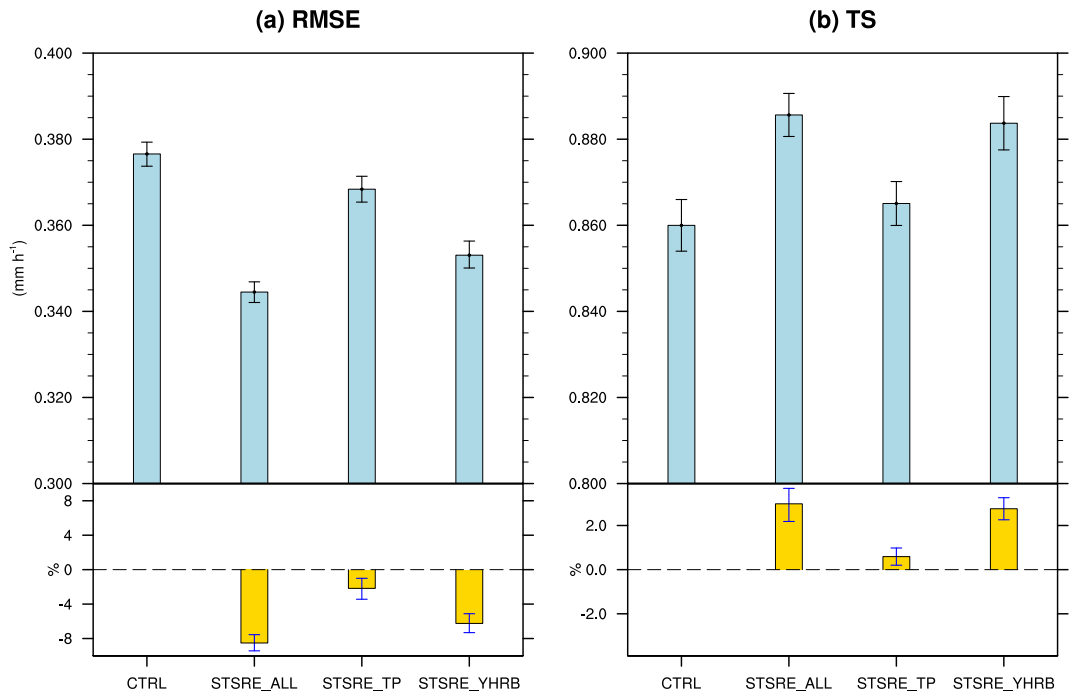

Figure 7. Domain-averaged RMSEs (a) and TSs (b) forecasted by the CTRL, STSRE_ALL, the STSRE_TP and the STSRE_YHRB experiments verified against observations (top panel in each sub-figure), with error bars representing two-tailed 90% confidence intervals over the Yangtze-Huaihe River Basin region, and the percentage changes produced by the STSRE_ALL, STSRE_TP and STSRE_YHRB experiments calculated at the 90% confidence interval (bottom panel in each sub-figure) relative to the CTRL experiment.

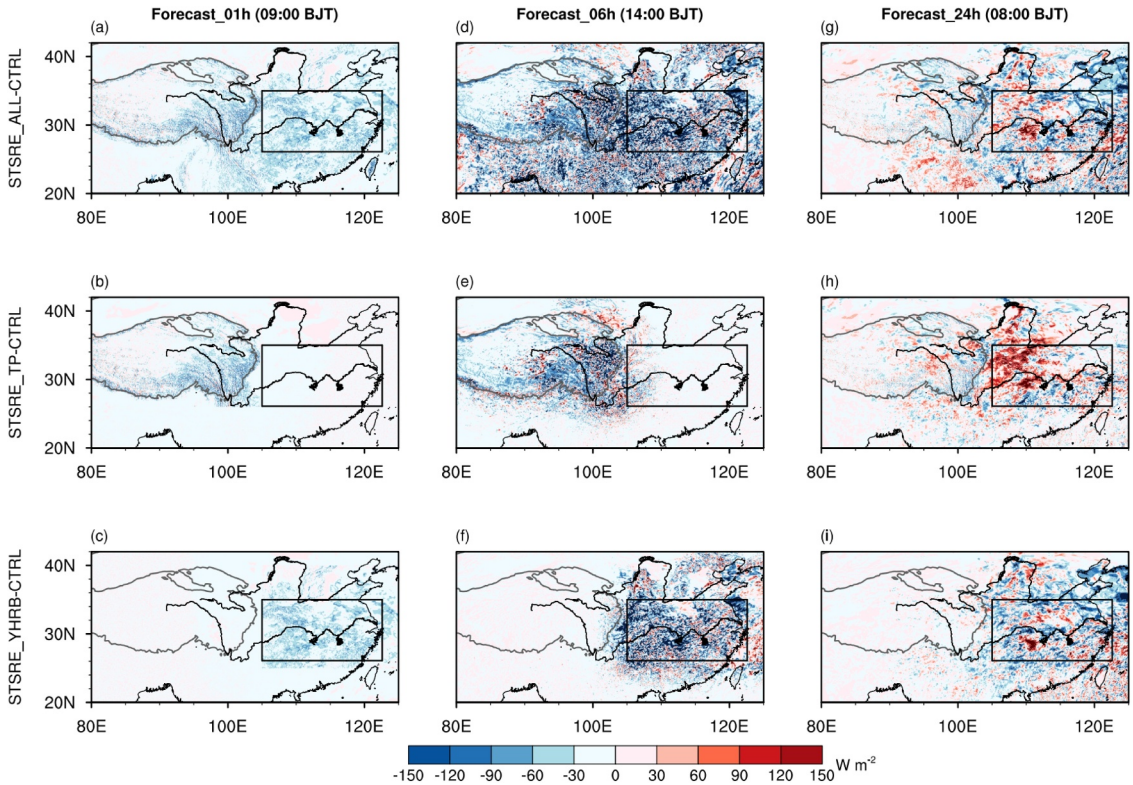

Figure 8. The differences in surface downward solar radiation between the STSRE_ALL and CTRL experiments (the first row), between the STSRE_TP and CTRL experiments (the second row), and between the STSRE_YHRB and CTRL experiments (the last row) at 09:00 BJT (the first hour forecast, the first column), 14:00 BJT (the sixth hour forecast, the second column) and 08:00 BJT (the 24th hour forecast, the last column) during three Meiyu rainfall events in June 2020. The gray lines denote the Tibetan Plateau region and the black lines indicate the Yangtze River and Yellow River. The black rectangles denote the Yangtze-Huaihe River Basin.

produced by each sensitive experiment relative to the CTRL experiment. In the first 1-hr forecast, the SDSR differences between the STSRE_ALL and CTRL experiments are mainly located in rugged areas with complex terrains, such as the southern and eastern edge of TP, the Hengduan mountainous regions and hilly area of eastern China, due to the strong STSRE in these regions (Figure 8a). Similarly, the relatively higher SDSR differences between the STSRE_TP (STSRE_YHRB) and CTRL experiments are limited to the rugged areas of the TP (YHRB) (Figures 8b and 8c). In the 6-hr forecast, the SDSR differences between the STSRE_ALL and CTRL experiments become much more noticeable and expand to almost the whole domain relative to the situations in the 1-hr forecast (Figure 8d). Likewise, as shown in Figures 8e and 8f, the SDSR differences between the STSRE_TP (STSRE_YHRB) and CTRL experiments become much higher and spread to the surrounding regions around the TP (YHRB). Overall, in the 6-hr forecast, most differences still stem from the local impact of STSRE on nearby terrains. It can be seen that the spatial distribution of SDSR differences between the STSRE_TP (STSRE_YHRB) and CTRL experiments is consistent with that over the TP (YHRB) in the STSRE_ALL experiment relative to the CTRL experiment (Figures 8d–8f).

It is not until 24-hr forecast that the SDSR differences caused by the remote STSRE in the TP spread to the YHRB (Figure 8h). Compared with the CTRL experiment, the STSRE_TP experiment increases the SDSR in most eastern China. The increase of SDSR is mainly originated from the eastern TP, which may be caused by the decrease of precipitation (Figure 6a) and clouds therein. The obvious SDSR differences between the STSRE_YHRB and CTRL experiments are still limited to the YHRB (Figure 8i), similar to the SDSR differences over the YHRB between the STSRE_ALL and CTRL experiments (Figure 8g). In the 30-hr forecast, the STSRE_ALL and STSRE_YHRB experiments both reduce the SDSR in the eastern China with a regionally mean decrease of -93.7 W m^{-2} and -103.1 W m^{-2}, respectively (figure not shown).

In short, the STSRE of the TP can remotely influence the SDSR in the downstream YHRB after a 24-hr forecast. While the STSRE in the YHRB first influences the local region, gradually spreading across East China through

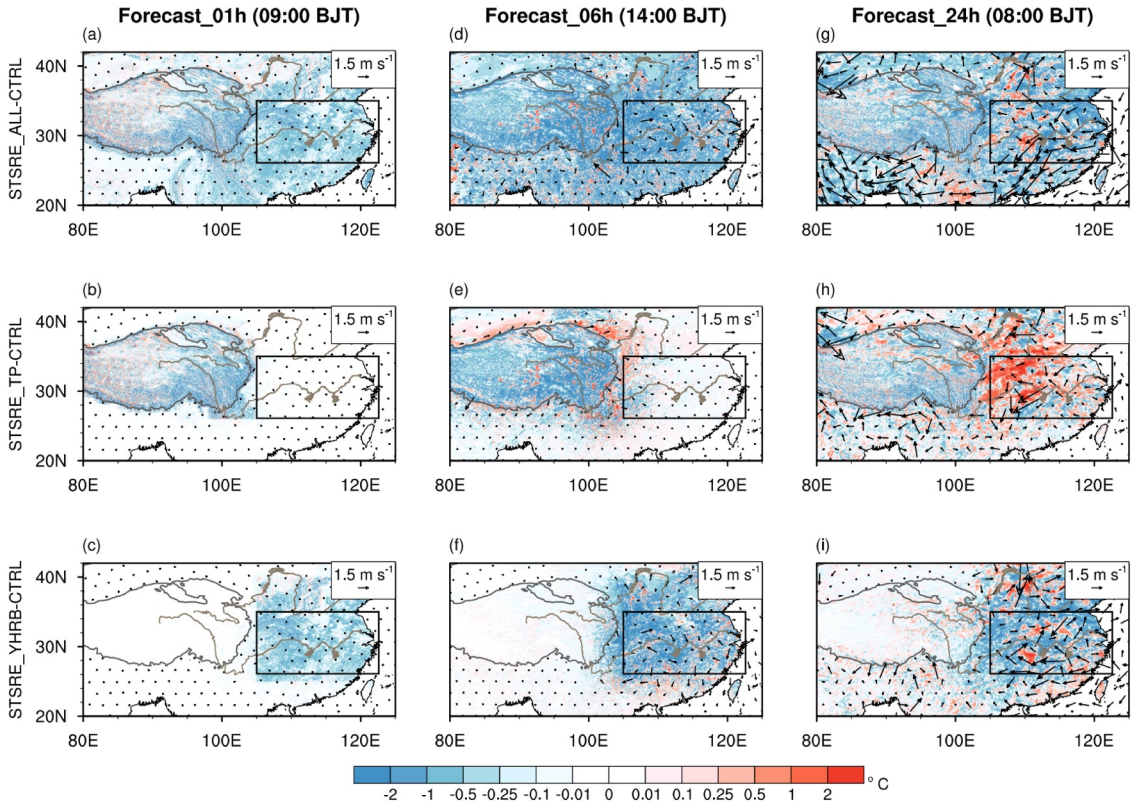

Figure 9. The differences in surface air temperature (shadings) and 850 hPa wind field (vectors) between the STSRE_ALL and CTRL experiments (the first row), between the STSRE_TP and CTRL experiments (the second row), and between the STSRE_YHRB and CTRL experiments (the last row) at 09:00 BJT (the first hour forecast, the first column), 14:00 BJT (the sixth hour forecast, the second column) and 08:00 BJT (the 24th hour forecast, the last column) during three Meiyu rainfall events in June 2020. The gray lines denote the Tibetan Plateau region and the light brown lines indicate the Yangtze River and Yellow River. The black rectangles denote the Yangtze-Huaihe River Basin.

integration. It has negligible impact on the upstream TP region. The SDSR changes can directly affect surface thermal properties through the surface energy balance process, subsequently altering the wind circulation patterns (Cai et al., 2023).

Figure 9 presents the differences of surface air temperature and 850 hPa wind field between each sensitive experiment and the CTRL experiment in different forecast time. The evolution of surface air temperature differences are consistent with the evolution of SDSR differences. In the 1-hr forecast, relatively higher negative surface air temperature differences between the STSRE_ALL experiment and CTRL experiment can be found only in the rugged regions (Figure 9a). Likewise, the surface air temperature differences only occur in the mountainous regions of the TP (YHRB) (Figures 9b and 9c). Meanwhile, the differences of low-level circulation between each sensitive experiment and the CTRL experiment are relatively weaker in the 1-hr forecast (Figures 9a–9c). In the 6-hr forecast, the magnitude of surface air temperature difference induced by the STSRE in all the sensitive experiments between the CTRL experiment increases and extends to surrounding regions. The 850 hPa wind differences induced by the STSRE also become apparent (Figures 9d–9f). In the 24-hr forecast, negative surface air temperature differences induced by the STSRE in both the STSRE_ALL and STSRE_YHRB experiments are located in the YHRB (Figures 9g and 9i). Meanwhile, the northeastern wind differences at 850 hPa between the STSRE_ALL and CTRL experiments are apparent in the YHRB, which attenuate the southwesterly moisture transport to the YHRB (Figure 9g). Likewise, the STSRE of the YHRB in the STSRE_YHRB experiment leads to northeastern wind differences there (Figure 9i). The STSRE of TP in the STSRE_TP experiment induces warm surface air temperature differences in the YHRB (Figure 9h), which correspond well with the SDSR differences (Figure 8h). Also, the remote STSRE of TP region weakly influences the low-level circulation in the Meiyu rainfall region at 24-hr forecast (Figure 9h). Overall, the 850 hPa wind differences between the STSRE_ALL and the CTRL experiment in the YHRB is mainly affected by the local

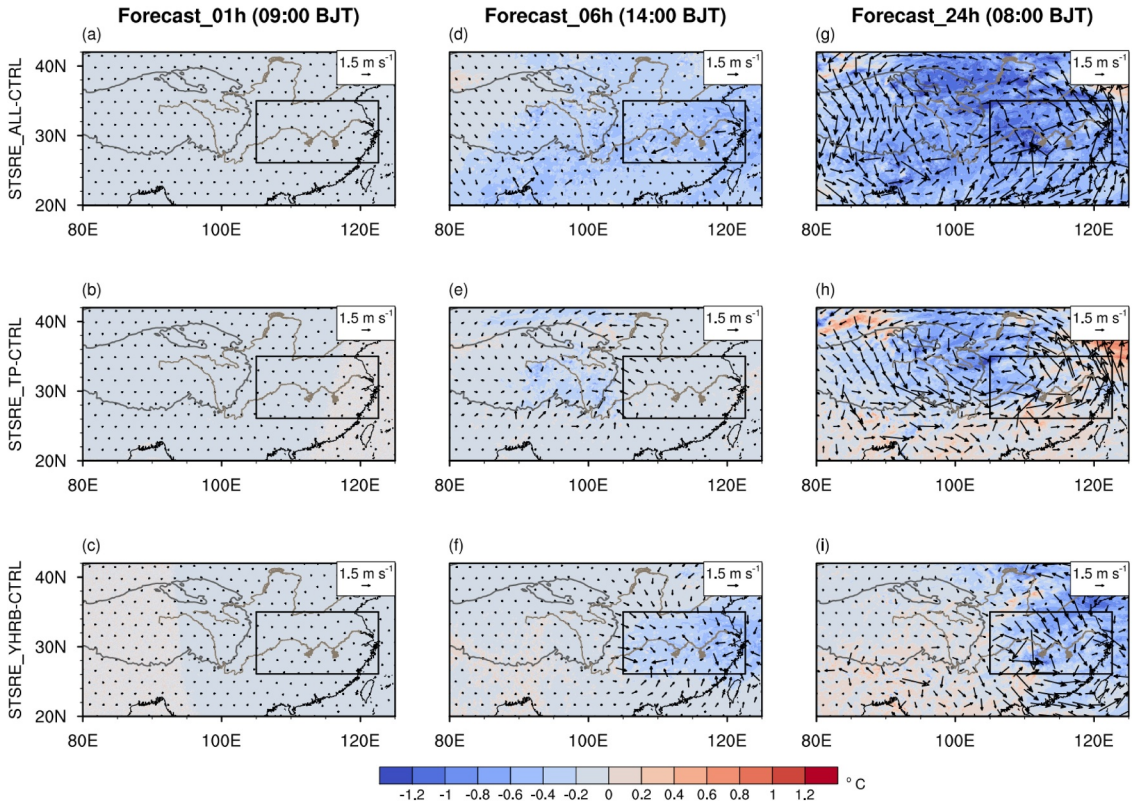

Figure 10. Same as Figure 9, but for the differences of 200 hPa air temperature (shading; units: ℃) and wind field (vector; units: m s^{-1}).

STSRE of YHRB, which can be identified by the differences between the STSRE_YHRB and CTRL experiments.

The above analysis mainly focuses on the impact of local and remote STSRE on the lower troposphere over YHRB. Apart from the impacts of the STSRE on the surface thermal condition and wind field in lower troposphere, the STSRE can also regulates the air temperature in the upper troposphere and circulations (Gu et al., 2020, 2022). Figure 10 displays the evolution of the 200 hPa air temperature and wind differences between each sensitive experiment and the CTRL experiment during the three Meiyu rainfall events in June 2020. In the 1-hr forecast, the 200 hPa air temperature and wind differences induced by the STSRE in the three sensitive experiments are very slight (Figures 10a–10c). In the 6-hr forecast, the STSRE leads to decreases in the 200 hPa air temperature over most areas (Figure 10d). Relatively more obvious cold differences induced by the STSRE of TP (YHRB) are located over the eastern TP (YHRB) (Figures 10e and 10f). In the 24-hr forecast, the air temperature and wind differences at 200 hPa between each sensitive experiment and the CTRL experiment become much more apparent with the forecast time increasing (Figures 10g–10i). A cyclonic circulation differences at 200 hPa induced by the STSRE of East Asia (TP) are located over the TP and YHRB (Figures 10g and 10h), implying weakening and westward shifting of the South Asian High. While the negative air temperature differences and anomalous cyclone difference at 200 hPa between the STSRE_YHRB and CTRL experiments are mainly located over the YHRB (Figure 10i).

From the above, the STSRE of the TP region can not only affect the local air temperature and circulation, but also has a remote impact on the air temperature and atmospheric circulations in the upper troposphere over downstream YHRB after 24-hr forecast. Yet the STSRE of the YHRB mainly influences the local surface thermal condition and the atmospheric circulations in the lower troposphere during the forecast time.

Figure 11 presents the mean differences in the SDSR, and the mean differences of the air temperature and atmospheric circulations in the lower and upper troposphere during the three Meiyu rainfall events in June 2020 between each sensitive experiment and the CTRL experiment. The negative SDSR differences induced by the STSRE in the STSRE_ALL experiment are evident in the Sichuan Basin and YHRB (Figure 2f). As for the

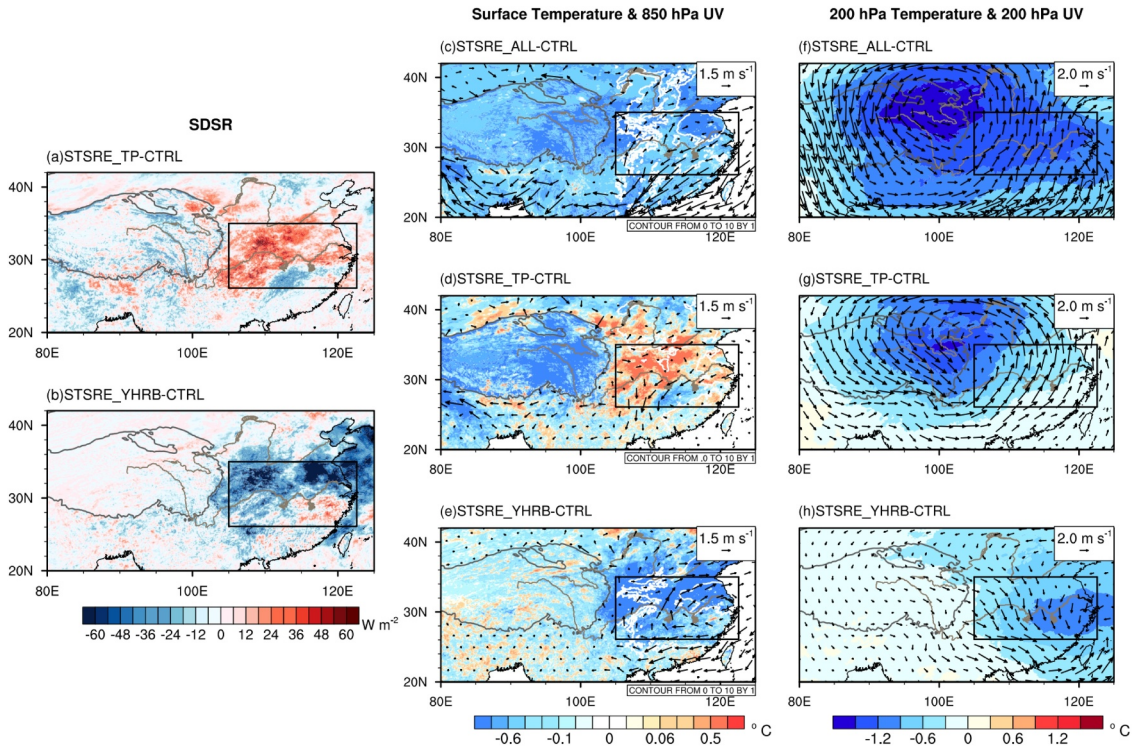

Figure 11. Mean differences of surface downward solar radiation between the STSRE_TP and CTRL experiments (a), and between STSRE_YHRB and CTRL experiments (b). Mean differences of surface air temperature (shadings) and 850 hPa wind field (vectors) between STSRE_ALL and CTRL experiments (c), STSRE_TP and CTRL experiments (d), and between STSRE_YHRB and CTRL experiments (e). Mean differences of 200 hPa air temperature (shadings) and wind field (vectors) between the STSRE_ALL and CTRL experiments (f), STSRE_TP and CTRL experiments (g), and between the STSRE_YHRB and CTRL experiments (h) during three Meiyu rainfall events in June 2020. The gray lines (light brown lines) denote the Tibetan Plateau region (the Yangtze River and Yellow River). The black rectangles denote the Yangtze-Huaihe River Basin. The white contours in (c)–(e) indicate the difference in surface pressure (>0, with contour interval of 1 hPa) between three experiments and CTRL experiment.

STSRE_TP experiment, the SDSR decreases in the TP while increases in the YHRB relative to the CTRL experiment (Figure 11a). In the STSRE_YHRB experiment, the negative SDSR differences induced by the STSRE of YHRB mainly concentrated in the YHRB (Figure 11b). As a whole, the STSRE of the TP can remotely affect the SDSR in its downstream YHRB. While the STSRE of the YHRB is merely limited to local impact on SDSR. By contrast, the negative SDSR differences in the YHRB induced by the STSRE of East Asia in the STSRE_ALL experiment are similar to those induced by the STSRE of YHRB in the STSRE_YHRB experiment, suggesting that the SDSR differences in the YHRB mainly comes from the local influence of STSRE in the YHRB.

The SDSR changes directly affect the surface thermal condition through the surface energy balance process. Hence, in the STSRE_ALL experiment, the surface air temperature over the YHRB decreases compared with CTRL (Figure 11c). This cooling aligns with the reduced SDSR shown in Figure 2f. The primary driver of the surface air temperature decline is the local STSRE within the YHRB (Figure 11e). The STSRE over the YHRB region generates a local cold high-pressure center (white contours) north of the Yangtze River (Figure 11e), which subsequently induces a local anticyclonic circulation anomaly in that area. East-northeasterly winds can be observed on the southern flank of this anticyclonic anomaly, weakening the southwesterly moisture transport there. Similarly, the 850 hPa wind difference between the STSRE_ALL and CTRL experiments also shows anomalous east-northeastward winds south of the Yangtze River, which inhibits the southwesterly moisture transport to the YHRB (Figure 11c). It should be noted that the remote STSRE over the TP region has minimal impact on the low-level circulation during the initial forecast period (Figures 9b, 9e, and 9h). After 36 hr, the local anticyclonic circulation anomaly driven by the STSRE_YHRB shifts eastward, inducing easterly wind differences. Meanwhile, the STSRE over the TP region weakens the South Asian High and induces a downward anomaly that propagates downstream (Figure not shown). This anomaly leads to airflow divergence toward the

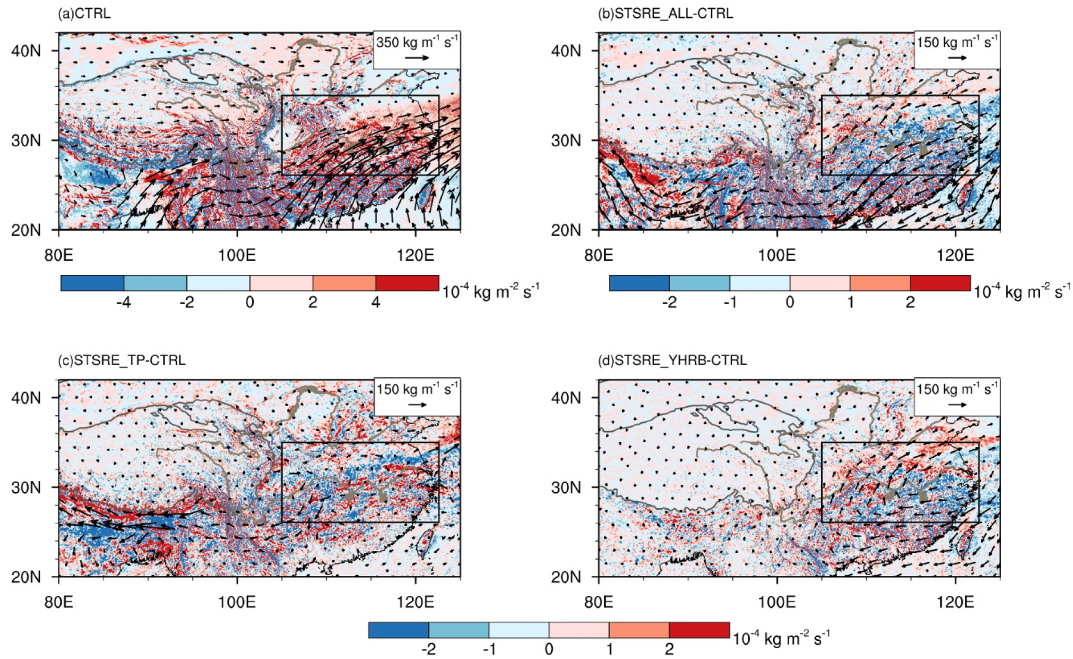

Figure 12. Mean water vapor transport flux (vectors) and its convergence (shadings) vertically integrated from the surface to 100 hPa during the three Meiyu rainfall events in June 2020 in the CTRL experiment (a), along with the differences between the STSRE_ALL and CTRL experiments (b), between the STSRE_TP and CTRL experiments (c), and between the STSRE_YHRB and CTRL experiments (d). The gray lines denote the Tibetan Plateau region and the light brown lines indicate the Yangtze River and Yellow River. The black rectangles denote the Yangtze-Huaihe River Basin.

surrounding regions and partially contributes to the northeasterly wind differences in southwest of the Meiyu rainfall region (Figure 11d).

In brief, the decrease in SDSR caused by local STSRE of the YHRB induces a surface cooling, generating a local cold anomaly and thereafter an anomalous anticyclone. This anticyclonic circulation then diminishes the southwesterly moisture transport, which directly alleviates the overestimation of Meiyu rainfall forecast. In contrast, the impact of TP STSRE gradually becomes apparent after 36-hr forecast, its influence is less pronounced than that of local STSRE.

In the upper troposphere, there exists a warm center at 200 hPa that is favorable for the maintenance of the South Asian high and airflow divergence (figure not shown). The STSRE in the STSRE_ALL experiment induces a strong cold difference at 200 hPa over almost the whole domain, attenuating the intensity of the warm center and South Asian High at 200 hPa. Affected by the weakened South Asian High, the circulation differences between the STSRE_ALL and the CTRL experiments presents an anomalous cyclone over the whole domain. Similarly, the STSRE of TP also induces negative air temperature differences and cyclonic wind differences at 200 hPa (Figures 11f and 11g). Hence, the 200 hPa air temperature and wind differences between the STSRE_ALL and CTRL experiments mainly come from the remote STSRE of the TP. In contrast, the 200 hPa air temperature and atmospheric circulation differences between the STSRE_YHRB and the CTRL experiments are mainly concentrated in YHRB, indicating the local impact of STSRE of YHRB (Figure 11h).

Figure 12 shows the mean vertically integrated moisture flux and its convergence from the CTRL experiment and the differences between each sensitive experiment and the CTRL experiment. During the three Meiyu rainfall events, strong southwesterly moisture transport and explicit moisture flux convergence can be found in the CTRL experiment over the YHRB (Figure 12a). Compared with the CTRL experiment, the STSRE_ALL and STSRE_YHRB experiments both decrease the convergence of airflow and attenuate the southwesterly water vapor transport over the YHRB (Figures 12b and 12d). Whereas the STSRE_TP experiment does not display explicit difference in the moisture flux convergence and transportation against the CTRL experiment. Hence, compared with the STSRE of TP, the STSRE of YHRB contributes more to the decreases in the column-

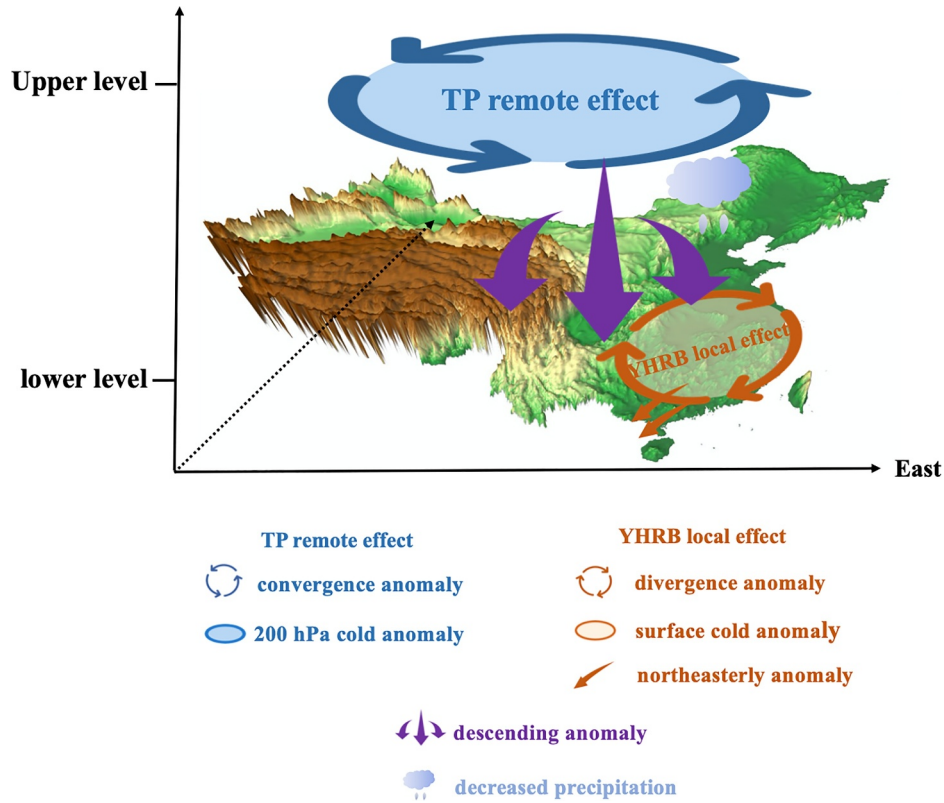

Figure 13. The conceptual figure of the main influences of remote in the Tibetan Plateau and local sub-grid terrain solar radiative effect in Yangtze-Huaihe River Basin on the Meiyu rainfall forecast.

integrated (surface to 100 hPa) water vapor transport flux and its convergence over the YHRB (Figures 12b and 12d). This is consistent with the results of precipitation evaluation in Figure 7.

Figure 13 displays the different impacts of STSRE of the TP and YHRB on Meiyu rainfall forecast. To sum up, the STSRE in the TP region influences the upper air temperature and circulation pattern at a regional scale (Figure 13). The air temperature and circulation deviations at 200 hPa over the YHRB are primarily caused by the remote influence of STSRE of TP. The remote STSRE of TP decreases the SDSR and modulates the radiative and heat fluxes between the land surface and the atmosphere, which leads to the attenuated warm center at 200 hPa across the entire China region, leading to weakened divergence at 200 hPa which impedes the development of the ascending motion over the YHRB (Figure 13). For the lower troposphere, although the remote STSRE over the TP partly contributes to the northeasterly wind anomaly at 850 hPa over the YHRB region after 36-hr forecast, the differences in air temperature and circulation at 850 hPa between the STSRE_ALL and CTRL experiments over the YHRB are mainly driven by the local STSRE. The decrease in near surface air temperature over the YHRB leads to a local cold anomaly and an anticyclonic circulation anomaly, which weakens the southwesterly water vapor transport there (Figure 13). The combined effects of the local and remote STSRE alleviate the overestimation of Meiyu rainfall forecast over the YHRB. Overall, the local STSRE in the YHRB contributes relatively more mitigation of the short-term Meiyu rainfall forecast.

5. Summary

The STSRE plays an important role in affecting local and remote land-atmosphere processes. This study addresses the impact of local and remote STSRE on the Meiyu rainfall forecast and the related mechanisms. Main findings are as follows:

The application of the 3D-STSRE scheme can relieve the overestimation of SDSR in the YHRB. The reduced SDSR directly affects the surface air temperature forecast and thereby influences wind circulation through surface energy balance processes. Corresponding to the weakened southwesterly wind induced by the STSRE, the

weakened moisture transport to the YHRB reduces the overestimation of Meiyu rainfall. Consideration of the 3D-STSRE in the whole model domain can lead to the RMSE of Meiyu rainfall forecast over the YHRB reduced by up to 10.43%. Moreover, the improvements are more significant as the forecast period extends.

Compared with the CTRL experiment, the decrease in the SDSR and the surface air temperature over the YHRB produced by the STSRE_ALL experiment is primarily attributed to the impact of local STSRE of the YHRB, which causes weakened surface thermal condition to activate a local anomalous anticyclonic circulation in the lower troposphere over the YHRB, leading to weakened southwesterly water vapor transport there and reduction of the overestimated Meiyu rainfall forecast. Although the remote STSRE of the TP begins to affect low-level wind circulation over the YHRB after a 36-hr forecast, its impact is still less significant than that of the local STSRE. In contrast, the differences of the air temperature and circulation in the upper troposphere over the YHRB between the STSRE_ALL and CTRL experiments are mainly induced by the remote impact of STSRE in the TP. The SDSR in TP reduced by the STSRE of TP weakens the atmospheric heating near the surface there. Consequently, the air temperature structure of the entire layer adjusts, exhibiting a weakened warm center and, thereby, a weakened South Asian High in the upper troposphere, leading to weakened divergence in the upper troposphere and suppressed ascending motion in the lower troposphere over the YHRB.

Overall, the combined influence of the STSRE in both TP and YRHB can mitigate the overestimation of Meiyu precipitation forecast. Compared with the TP, although the terrain of the YHRB is relatively flatter, the local STSRE of YHRB can lead to much larger improvement of the Meiyu rainfall forecast over the YHRB for 3–4 days short-range weather forecasts.

This study only provides a method to alleviate Meiyu rainfall bias by depicting more realistic terrain and land-air interactions. In fact, many factors may influence Meiyu rainfall forecasts. For example, studies show that most microphysics parameterizations fail to accurately represent microphysical characteristics (e.g., droplet size and number concentration), ultimately resulting in high precipitation forecast biases, especially for extreme rainfall events (Chen et al., 2023; Zhu et al., 2023). In future work, other potential solutions will be tested.

Conflict of Interest

The authors declare no conflicts of interest relevant to this study.

Data Availability Statement

Datasets: (a) The shortwave downwelling radiation observation data (Letu et al., 2022) was used for the evaluation of surface downward solar radiation. (b) The Meiyu precipitation forecasts were validated against the gauge-satellite merged observation data set (Shen et al., 2014). (c) NCEP Global Forecast System (NCEP-GFS) real-time forecast data (NCEP, 2015) was used to provide the initial and boundary conditions for the Meiyu rainfall forecast. (d) The 3″ (∼90 m) digital elevation data (Jarvis et al., 2008) was used to derive the sub-grid terrain parameters. Software: The codes of WRF_CPM coupled with 3D-STSRE scheme were made available through Zenodo (Cai, 2023).

Acknowledgments
Our work is sponsored by the National Natural Science Foundation of China under Grant U2342207, 42475161 and 42375157, the Jiangsu University "Blue Project" outstanding young teachers training object, the Jiangsu Collaborative Innovation Center for Climate Change. We express the gratitude to the High-Performance Computing Center of Nanjing University.

References

Cai, S. (2023). WRF-3D STSRE [Software]. *Zenodo*. https://doi.org/10.5281/zenodo.7722215

Cai, S., Huang, A., Zhu, K., Guo, W., Wu, Y., & Gu, C. (2023). The forecast skill of the summer precipitation over Tibetan plateau improved by the adoption of a 3D sub-grid terrain solar radiative effect scheme in a convection-permitting model. *Journal of Geophysical Research: Atmospheres*, *128*(11), e2022JD038105. https://doi.org/10.1029/2022JD038105

Cai, S., Huang, A., Zhu, K., Yang, B., Yang, X., Wu, Y., & Mu, X. (2021). Diurnal cycle of summer precipitation over the Eastern Tibetan Plateau and surrounding regions simulated in a convection-permitting model. *Climate Dynamics*, *57*(1), 611–632. https://doi.org/10.1007/s00382-021-05729-5

Chen, F., & Dudhia, J. (2001). Coupling an advanced land surface–hydrology model with the Penn State–NCAR MM5 modeling system. Part I: Model implementation and sensitivity. *Monthly Weather Review*, *129*(4), 569–585. https://doi.org/10.1175/1520-0493(2001)129<0569:CAALSH>2.0.CO;2

Chen, G., Lu, Y., Hua, S., Liu, Q., Zhao, K., Zheng, Y., et al. (2023). Evaluating the variability of simulated raindrop size distributions in the "21·7" Henan extremely heavy rainfall event. *Geophysical Research Letters*, *50*(8), e2023GL102849. https://doi.org/10.1029/2023GL102849

Chen, Y., Li, Y., & Zhao, T. (2015). Cause analysis on eastward movement of Southwest China vortex and its induced heavy rainfall in South China. *Advances in Meteorology*, *2015*, 1–22. https://doi.org/10.1155/2015/481735

Collins, W. D., Rasch, P. J., Boville, B. A., Hack, J. J., McCaa, J. R., Williamson, D. L., et al. (2004). Description of the NCAR community atmosphere model (CAM 3.0). *NCAR Tech. Note NCAR/TN-464+ STR*, *226*, 1326–1334. https://doi.org/10.5065/D63N21CH

Ding, Y. (1992). Summer monsoon rainfalls in China. *Journal of the Meteorological Society of Japan. Ser. II*, *70*(1B), 373–396. https://doi.org/10.2151/jmsj1965.70.1B_373

Ding, Y., & Chan, J. C. L. (2005). The East Asian summer monsoon: An overview. *Meteorology and Atmospheric Physics*, *89*(1), 117–142. https://doi.org/10.1007/s00703-005-0125-z

Ding, Y., Liu, Y., & Hu, Z. Z. (2021). The record-breaking Meiyu in 2020 and associated atmospheric circulation and tropical SST anomalies. *Advances in Atmospheric Sciences*, *38*(12), 1980–1993. https://doi.org/10.1007/s00376-021-0361-2

Duan, A., Wu, G., Liu, Y., Ma, Y., & Zhao, P. (2012). Weather and climate effects of the Tibetan Plateau. *Advances in Atmospheric Sciences*, *29*(5), 978–992. https://doi.org/10.1007/s00376-012-1220-y

Gu, C., Huang, A., Li, X., & Wu, Y. (2024). Offline correction of CMIP6 HighResMIP simulated surface solar irradiance with 3D sub-grid terrain radiative effects. *Geophysical Research Letters*, *51*(10), e2023GL107737. https://doi.org/10.1029/2023GL107737

Gu, C., Huang, A., Wu, Y., Yang, B., Mu, X., Zhang, X., & Cai, S. (2020). Effects of sub grid terrain radiative forcing on the ability of RegCM4.1 in the simulation of summer precipitation over China. *Journal of Geophysical Research: Atmospheres*, *125*(12), e2019JD032215. https://doi.org/10.1029/2019jd032215

Gu, C., Huang, A., Zhang, Y., Yang, B., Cai, S., Xu, X., et al. (2022). The wet bias of RegCM4 over Tibet Plateau in summer reduced by adopting the 3D sub-grid terrain solar radiative effect parameterization scheme. *Journal of Geophysical Research: Atmospheres*, *127*(21), e2022JD037434. https://doi.org/10.1029/2022JD037434

Guo, Z., Fang, J., Sun, X., Tang, J., Yang, Y., & Tang, J. (2020). Decadal long convection-permitting regional climate simulations over eastern China: Evaluation of diurnal cycle of precipitation. *Climate Dynamics*, *54*(3), 1329–1349. https://doi.org/10.1007/s00382-019-05061-z

Hao, D., Bisht, G., Gu, Y., & Leung, L. R. (2023). Regional and teleconnected impacts of solar radiation-topography interaction over the Tibetan Plateau. *Geophysical Research Letters*, *50*(23), e2023GL106293. https://doi.org/10.1029/2023GL106293

Hong, S. Y., Dudhia, J., & Chen, S. H. (2004). A revised approach to ice microphysical processes for the bulk parameterization of clouds and precipitation. *Monthly Weather Review*, *132*(1), 103–120. https://doi.org/10.1175/1520-0493(2004)132<0103:ARATIM>2.0.CO;2

Hong, S. Y., Noh, Y., & Dudhia, J. (2006). A new vertical diffusion package with an explicit treatment of entrainment processes. *Monthly Weather Review*, *134*(9), 2318–2341. https://doi.org/10.1175/MWR3199.1

Hu, Y., Zhu, X., Ha, Y., Zhu, Y., & Zhong, Z. (2024). Another source of error in simulating or predicting Meiyu: A case study. *Theoretical and Applied Climatology*, *155*(12), 1–14. https://doi.org/10.1007/s00704-024-05218-9

Huang, A., Gu, C., Zhang, Y., Li, W., Zhang, L., Wu, Y., et al. (2022). Development of a clear-sky 3D sub-grid terrain solar radiative effect parameterization scheme based on the mountain radiation theory. *Journal of Geophysical Research: Atmospheres*, *127*(13), e2022JD036449. https://doi.org/10.1029/2022JD036449

Jarvis, A., Reuter, H. I., Nelson, A., & Guevara, E. (2008). Hole-filled SRTM for the globe version 4 [Dataset]. *International Centre for Tropical Agriculture (CIAT)*. Retrieved from http://srtm.csi.cgiar.org

Jin, E. K., Choi, I. J., Kim, S. Y., & Han, J. Y. (2016). Impact of model resolution on the simulation of diurnal variations of precipitation over East Asia. *Journal of Geophysical Research: Atmospheres*, *121*(4), 1652–1670. https://doi.org/10.1002/2015JD023948

Joyce, R. J., Janowiak, J. E., Arkin, P. A., & Xie, P. (2004). CMORPH: A method that produces global precipitation estimates from passive microwave and infrared data at high spatial and temporal resolution. *Journal of Hydrometeorology*, *5*(3), 487–503. https://doi.org/10.1175/1525-7541(2004)005<0487:CAMTPG>2.0.CO;2

Lee, W. L., Liou, K. N., Wang, C. C., Gu, Y., Hsu, H. H., & Li, J. L. F. (2019). Impact of 3-D radiation-topography interactions on surface temperature and energy budget over the Tibetan plateau in winter. *Journal of Geophysical Research: Atmospheres*, *124*(3), 1537–1549. https://doi.org/10.1029/2018JD029592

Letu, H., Nakajima, T. Y., Wang, T., Shang, H., Ma, R., Yang, K., et al. (2022). A new benchmark for surface radiation products over the East Asia–Pacific region retrieved from the Himawari-8/AHI next-generation geostationary satellite [Dataset]. *Bulletin of the American Meteorological Society*, *103*(3), E873–E888. https://doi.org/10.1175/BAMS-D-20-0148.1

Li, P., Furtado, K., Zhou, T., Chen, H., & Li, J. (2021). Convection-permitting modelling improves simulated precipitation over the central and eastern Tibetan Plateau. *Quarterly Journal of the Royal Meteorological Society*, *147*(734), 341–362. https://doi.org/10.1002/qj.3921

Li, P., Furtado, K., Zhou, T., Chen, H., Li, J., Guo, Z., & Xiao, C. (2020). The diurnal cycle of East Asian summer monsoon precipitation simulated by the met office unified model at convection-permitting scales. *Climate Dynamics*, *55*(1–2), 131–151. https://doi.org/10.1007/s00382-018-4368-z

Luo, Y., & Chen, Y. (2015). Investigation of the predictability and physical mechanisms of an extreme-rainfall-producing mesoscale convective system along the Meiyu front in East China: An ensemble approach. *Journal of Geophysical Research: Atmospheres*, *120*(20), 10–593. https://doi.org/10.1002/2015JD023584

Ma, Y., Hu, Z., Xie, Q., Meng, X., Zhao, L., & Dong, W. (2022). Convection-permitting modeling over the Tibetan Plateau improves the simulation of Meiyu rainfall during the 2011 Yangtze Plain flood. *Atmospheric Research*, *265*, 105907. https://doi.org/10.1016/j.atmosres.2021.105907

NCEP. (2015). NCEP GFS 0.25° global forecast grids historical archive [Dataset]. Retrieved from https://rda.ucar.edu/datasets/ds084.1/

Pan, Y., Zhu, K., Xue, M., Wang, X., Hu, M., Benjamin, S. G., et al. (2014). A GSI-based coupled EnSRF–En3DVar hybrid data assimilation system for the operational Rapid refresh model: Tests at a reduced resolution. *Monthly Weather Review*, *142*(10), 3756–3780. https://doi.org/10.1175/MWR-D-13-00242.1

Shen, Y., Zhao, P., Pan, Y., & Yu, J. (2014). A high spatiotemporal gauge-satellite merged precipitation analysis over China [Dataset]. *Journal of Geophysical Research: Atmospheres*, *119*(6), 3063–3075. https://doi.org/10.1002/2013JD020686

Shi, W., Zhu, K., Li, X., & Zhang, B. (2024). Evaluation of precipitation forecast by the operational China meteorological administration mesoscale model during the 2020 Meiyu period. *Journal of Geophysical Research: Atmospheres*, *129*(11), e2023JD039156. https://doi.org/10.1029/2023JD039156

Shi, X., & Wen, M. (2015). Distribution and variation of persistent heavy rainfall events in China and possible impacts of heating source anomaly over Qinghai-Xizang Plateau. *Plateau Meteorology*, *34*(3), 611–620. (in Chinese).

Tao, S., & Chen, L. (1987). A review of recent research on the East Asian summer monsoon in China. In C. P. Chang & T. N. Krishnamurti (Eds.), *Monsoon meteorology* (pp. 60–92). Oxford University Press.

Taylor, K. E. (2001). Summarizing multiple aspects of model performance in a single diagram. *Journal of Geophysical Research*, *106*(D7), 7183–7192. https://doi.org/10.1029/2000JD900719

Wang, B., Liu, J., Yang, J., Zhou, T., & Wu, Z. (2009). Distinct principal modes of early and late summer rainfall anomalies in East Asia. *Journal of Climate*, *22*(13), 3864–3875. https://doi.org/10.1175/2009JCLI2850.1

Wu, G., Liu, Y., Zhang, Q., Duan, A., Wang, T., Wan, R., et al. (2007). The influence of mechanical and thermal forcing by the Tibetan Plateau on Asian climate. *Journal of Hydrometeorology*, *8*(4), 770–789. https://doi.org/10.1175/JHM609.1

Wu, G., Ma, T., Liu, Y., & Jiang, Z. (2020). PV-Q perspective of cyclogenesis and vertical velocity development downstream of the Tibetan Plateau. *Journal of Geophysical Research: Atmospheres*, *125*(16), e2019JD030912. https://doi.org/10.1029/2019JD030912

Wu, Q., Luo, T., & Hong, J. (2025). Incorporating hourly convective cloud data into tropical cyclone rapid intensification forecasting with machine learning. *Journal of Geophysical Research: Machine Learning and Computation*, *2*(1), e2025JH000595. https://doi.org/10.1029/2025JH000595

Wu, Y., Huang, A., Huang, D., Chen, F., Yang, B., Zhou, Y., et al. (2018). Diurnal variations of summer precipitation over the regions east to Tibetan Plateau. *Climate Dynamics*, *51*(11), 4287–4307. https://doi.org/10.1007/s00382-017-4042-x

Xu, J., Tao, J., & Xia, J. (2000). A meso-scale analysis of Qinghai-Xizang Plateau snow storm and its vortex source study. *Plateau Meteor*, *19*(2), 187–197. (in Chinese).

Xu, M., Zhao, C., Gu, J., Feng, J., Hagos, S., Leung, L. R., et al. (2021). Convection-permitting hindcasting of diurnal variation of Meiyu rainfall over East China with a global variable-resolution model. *Journal of Geophysical Research: Atmospheres*, *126*(14), e2021JD034823. https://doi.org/10.1029/2021JD034823

Xu, X., Lu, C., Shi, X., & Ding, Y. (2010). Large-scale topography of China: A factor for the seasonal progression of the Meiyu rainband? *Journal of Geophysical Research*, *115*(D2), D02110. https://doi.org/10.1029/2009JD012444

Xu, X., Zhou, M., Chen, J., Bian, L., Zhang, G., Liu, H., et al. (2002). A comprehensive physical pattern of land-air dynamic and thermal structure on the Qinghai-Xizang Plateau. *Science in China - Series D: Earth Sciences*, *45*(7), 577–594. https://doi.org/10.1360/02yd9060

Xue, M., Luo, X., Zhu, K., Sun, Z., & Fei, J. (2018). The controlling role of boundary layer inertial oscillations in Meiyu frontal precipitation and its diurnal cycles over China. *Journal of Geophysical Research: Atmospheres*, *123*(10), 5090–5115. https://doi.org/10.1029/2018JD028368

Yu, B., Zhu, K., Xue, M., & Zhou, B. (2020). Using new neighborhood-based intensity-scale verification metrics to evaluate WRF precipitation forecasts at 4 and 12 km grid spacings. *Atmospheric Research*, *246*, 105117. https://doi.org/10.1016/j.atmosres.2020.105117

Yun, Y., Liu, C., Luo, Y., Liang, X., Huang, L., Chen, F., & Rasmmusen, R. (2020). Convection-permitting regional climate simulation of warm-season precipitation over Eastern China. *Climate Dynamics*, *54*(3), 1469–1489. https://doi.org/10.1007/s00382-019-05070-y

Zeng, W., Chen, G., Bai, L., Liu, Q., & Wen, Z. (2022). Multiscale processes of heavy rainfall over East Asia in summer 2020: Diurnal cycle in response to synoptic disturbances. *Monthly Weather Review*, *150*(6), 1355–1376. https://doi.org/10.1175/MWR-D-21-0308.1

Zhang, X., Huang, A., Dai, Y., Li, W., Gu, C., Yuan, H., et al. (2022). Influences of 3D sub-grid terrain radiative effect on the performance of CoLM over Heihe River Basin, Tibetan plateau. *Journal of Advances in Modeling Earth Systems*, *14*(1), e2021MS002654. https://doi.org/10.1029/2021MS002654

Zhang, X., Huang, A., Yang, X., Gu, C., Cai, S., & Luo, J. (2024). Performance of common land model in simulating the land surface thermal and hydrological processes over China improved by including the sub-grid terrain solar radiative effect. *Journal of Geophysical Research: Atmospheres*, *129*(24), e2023JD039775. https://doi.org/10.1029/2023JD039775

Zhu, K., Xue, M., Yang, N., & Zhang, C. (2023). How well does 4-km WRF model predict three-dimensional reflectivity structure over China as compared to radar observations? *Journal of Geophysical Research: Atmospheres*, *128*(7), e2022JD038143. https://doi.org/10.1029/2022JD038143

Zhu, K., Xue, M., Zhou, B., Zhao, K., Sun, Z., Fu, P., et al. (2018). Evaluation of real-time convection-permitting precipitation forecasts in China during the 2013–2014 summer season. *Journal of Geophysical Research: Atmospheres*, *123*(2), 1037–1064. https://doi.org/10.1002/2017JD027445

Zhu, K., Yu, B., Xue, M., Zhou, B., & Hu, X. (2021). Summer season precipitation biases in 4 km WRF forecasts over southern China: Diagnoses of the causes of biases. *Journal of Geophysical Research: Atmospheres*, *126*(23), e2021JD035530. https://doi.org/10.1029/2021JD035530